Quantitative Assessment of Dynamic Stability Characteristics for Jet Transport in Sudden Plunging Motion

Yonghu Wang (wangyonghu@cqjtu.edu.cn)
College of Aeronautics, Chongqing Jiaotong Unversity
Ray C. Chang
Changzhou Institute of Technology
Wei Jiang
Changzhou Institute of Technology

Research Article

Keywords: plunging motion, clear-air turbulence, stability characteristics, motion modes, eigenvalues

Posted Date: December 28th, 2021

DOI: https://doi.org/10.21203/rs.3.rs-1194701/v1

Quantitative Assessment of Dynamic Stability Characteristics for Jet Transport in Sudden Plunging Motion

Abstract

The main objective of this article is to present a training program of loss control prevention for the airlines to enhance aviation safety and operational efficiency. The assessments of dynamic stability characteristics based on the approaches of oscillatory motion and eigenvalue motion modes for jet transport aircraft response to sudden plunging motions are demonstrated in this article. A twin-jet transport aircraft encountering severe clear-air turbulence in transonic flight during the descending phase will be examined as the study case. The flight results in sudden plunging motions with abrupt changes in attitude and gravitational acceleration (i.e. the normal load factor). Development of the required thrust and aerodynamic models with the flight data mining and the fuzzy-logic modeling techniques will be presented. The oscillatory derivatives extracted from these aerodynamic models are then used in the study of variations in stability characteristics during the sudden plunging motion. The fuzzy-logic aerodynamic models are utilized to estimate the nonlinear unsteady aerodynamics while performing numerical integration of flight dynamic equations. The eigenvalues of all motion modes are obtained during time integration. The present quantitative assessment method is an innovation to examine possible mitigation concepts of accident prevention and promote the understanding of aerodynamic responses of the jet transport aircraft.

Keywords: plunging motion, clear-air turbulence, stability characteristics; motion modes; eigenvalues

Introduction

The databases of flight simulators and autopilots are designed and established based on data in nominal flights in current state of art. The flight condition of transport aircraft does not include in normal design process and this situation cannot be tested easily during the aircraft certification process, but most likely to cause the aircraft loss of control in service is so-called off-nominal condition. The flight mechanism of off-nominal condition cannot be simulated by wind tunnel tests easily, and it is not possible to directly perform flight tests with real aircraft. In other words, the design value of aerodynamic performance is not consistent with the actual aerodynamic performance during the flight operations. It is appropriate that off-nominal flight conditions cannot be combined with aircraft design and flight simulators (Chang and Tan 2013). More importantly, the pilots can't have much chance to hone in this flight condition.

The adverse weather related to off-nominal flight conditions include (but are not limited to): Heavy rain, convective storms (Sauer et al. 2019), turbulence (Hamilton and Proctor 2003; Lee and Lan 2000), crosswind (Lan and Chang 2018; Weng et al. 2006), wind shear (Min et al. 2011; Wang et al. 2016), in-flight icing (Lan and Guan 2005; Thompson et al. 2004). Adverse weather impacts the flight safety of transport aircraft and operational efficiency of air traffic management. An innovation tool of commercial flight route planning program is developed to avoid the deep convective storms (Sauer et al. 2019). This program provides an overview to make a better air route based on original trajectory operations for safe, efficient, and comfortable operating flights to the airlines.

Among the different adverse weathers, clear-air turbulence is all the more important in-flight safety since it is hard to detect and predict. Clear-air turbulence is the leading cause of serious personal injuries in non-fatal accidents of commercial aircraft. One main type of motion that causes flight injuries in clear-air turbulence is the sudden plunging motion with abrupt changes in attitude and gravitational acceleration (i.e. the normal load factor). The assessment of flying qualities during sudden plunging motion for an aged twin-jet transport aircraft encountering severe clear-air turbulence through digital 6-DOF flight simulations in transonic flight was presented in reference (Chang et al. 2009). To numerically integrate the 6-DOF dynamic equations of motion and determine

the eigen-modes of motion at the same time at every instant were the important process of that approach. The longitudinal equations being coupled with the lateral-directional equations and some nonlinear effects being incorporated were the advantages for 6-DOF flight simulations. The eigenvalue equations were solved with QR transformation (Chang et al. 2009). Unfortunately, that approach was difficult to identify the individual modes of motion from these eigenvalues, from one instant, to another because of the rapid changes of aerodynamic forces and moments in turbulence.

To have a better approach, this article presents flight data mining and the fuzzy-logic modeling of artificial intelligence technique to establish nonlinear and unsteady aerodynamic models for six aerodynamic coefficients based on the flight data of a new twin-jet transport aircraft. This new twin-jet encountered severe clear-air turbulence twice during the descending phase. The oscillatory derivatives extracted from the aerodynamic models are then used in the study of variations in stability characteristics during the sudden plunging motion. The longitudinal and lateral-directional motion modes are analyzed through digital flight simulation based on decoupled dynamic equations of motion. The eigenvalue equations are formulated in the form of polynomials and solved. The eigenvalues for short-period, phugoid (long-period), dutch roll, spiral, and roll modes of motion are estimated based on damping ratio and undamped natural frequency. A positive real part of the eigenvalues is to indicate unstable motion of the related modes. The evaluations of unstable conditions for each eigen mode with the oscillatory derivatives are also demonstrated in the present paper.

Flight Data Mining Technology

The input data for fuzzy-logic modeling is extracted from post-flight data. There are many flight parameters recorded by QAR, but some of them are not related to the current study, such as light signs, landing gear retracting, ..., etc.. The steps are to collect and organize a large amount of data and obtain the required information from them for specific analysis and applications; this process is so called flight data mining (Han et al. 2011). The flight data mining process is divided into two parts: the developments of a non-linear and unsteady aerodynamic database and the aerodynamic models.

Development of nonlinear and unsteady aerodynamic database

This section describes the development process of the demand data selection, data frequency upscaling and data make up, compatibility check, and input information of aircraft main geometry and moment of inertia data. The flowchart of each step is shown in Fig. 2.1.

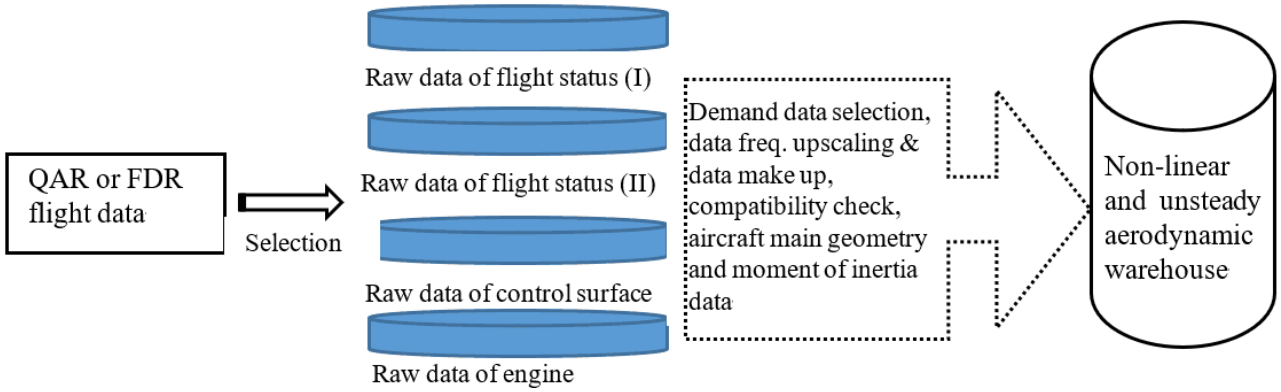

Fig. 2.1 Flowchart for development of a non-linear and unsteady aerodynamic data database

Before developing a non-linear and unsteady aerodynamic database, one must ensure that the selected parameters and corresponding data are the required data for study. The parameters and corresponding data required for current study include the following items:

1) To select the required flight status, flight control surface, and engine raw data for a specific flight number from the actual flight QAR or FDR data.
2) The main geometric and moment of inertial data include appearance size, wingspan, average chord length, and wing area, etc.. Most of the above are public data of aircraft manufacturers and can be obtained via the Internet. However, the thrust performance of the entire aircraft is non-public data and must be obtained from the Flight Planning and Performance Manual (Boeing Series) or Flight Crew Operation Manual (Airbus Series).

The frequency of each parameter sensor is different from 1Hz to 8Hz due to the properties and characteristics of the parameters. For example, attitude angles such as roll, pitch, and heading angles are 4Hz; aileron and elevator angles are 2Hz; the vertical acceleration sampling rate is 8Hz. To preserve the properties and characteristics of each parameter, it is necessary to avoid high frequency data loss, so the frequency of all original data sampling is uniformly arranged to 8 Hz.

The data frequency increase and data make up of this research is developed based on the method

of monotone cubic spline interpolation (Wolberg and Alfy 2002). This method is commonly used in aircraft flight test analysis to provide a smooth curve. Data upscaling and data completion of blanks are important steps for aerodynamic database to have high accuracy and reliability in applications to operational efficiency enhancement of transport aircraft.

Compatibility Check

Typically, the longitudinal, lateral, and vertical accelerations (a_x, a_y, a_z) along the (x, y, z)-body axes of aircraft, angle of attack α, Euler angles (ϕ, θ, and ψ), aileron deflection (δ_a), elevator (δ_e), rudder (δ_r), stabilizer (δ_s), …, etc. are available and recorded in the QAR of all transport aircraft. Since the recorded flight data may contain errors (or called biases), compatibility checks are performed to remove them by satisfying the following kinematic equations (Lan and Chang 2012; Lan et al. 2012):

$$\dot{\phi} = p + q\sin\phi\tan\theta + r\cos\phi\tan\theta \tag{2.1}$$

$$\dot{\theta} = q\cos\phi - r\sin\phi \tag{2.2}$$

$$\dot{\psi} = (q\sin\phi + r\cos\phi)\sec\theta \tag{2.3}$$

$$\begin{aligned}\dot{V} &= (a_x - g\sin\theta)\cos\alpha\cos\beta + (a_y + g\sin\phi\cos\theta)\sin\beta \\ &+ (a_z + g\cos\phi\cos\theta)\sin\alpha\cos\beta\end{aligned} \tag{2.4}$$

$$\begin{aligned}\dot{\alpha} &= [(a_z + g\cos\theta\cos\phi)\cos\alpha - (a_x - g\sin\theta)\sin\alpha]/(V\cos\beta) \\ &+ q - \tan\beta(p\cos\alpha + r\sin\alpha)\end{aligned} \tag{2.5}$$

$$\begin{aligned}\dot{\beta} &= \cos\beta(a_y + g\cos\theta\sin\phi)/V + p\sin\alpha - r\cos\alpha \\ &- \sin\beta[(a_z + g\cos\theta\cos\phi)\sin\alpha - (a_x - g\sin\theta)\cos\alpha]/V\end{aligned} \tag{2.6}$$

where g is the gravitational acceleration and V is the flight speed. Let the errors be denoted by $b_{a_x}, b_{a_y}, b_{a_z}, b_p, b_q, b_r, b_V, b_\alpha, b_\beta, b_\theta, b_\phi, b_\psi$, respectively for a_x, a_y, a_z, etc. These errors are estimated by minimizing the squared sum of the differences between the two sides of Eqs. 2.1~2.6.

These equations in vector form can be written as:

$$\dot{\vec{z}} = \vec{f}(\vec{x}) = \vec{f}(\vec{x}_m - \Delta\vec{x}) \tag{2.7}$$

where

$$\vec{z} = (V, \overline{\alpha}, \overline{\beta}, \theta, \phi, \psi)^T \tag{2.8}$$

$$\vec{x}_m = (\bar{a}_x, \bar{a}_y, \bar{a}_z, \bar{p}, \bar{q}, \bar{r}, V, \bar{\alpha}, \bar{\beta}, \theta, \phi, \psi)^T \tag{2.9}$$

$$\Delta\vec{x} = (b_{a_x}, b_{a_y}, b_{a_z}, b_p, b_q, b_r, b_V, b_\alpha, b_\beta, b_\theta, b_\phi, b_\varphi)^T \tag{2.10}$$

where super fix " - " stands for the mean value and the subscript "m" indicates the measured or recorded values. The cost function is defined as:

$$J = \frac{1}{2}(\dot{\vec{z}} - \vec{f})^T Q(\dot{\vec{z}} - \vec{f}) \tag{2.11}$$

where Q is a weighting diagonal matrix with elements being 1.0 and $\dot{\vec{z}}$ is calculated with a central difference scheme with $\vec{z}_m$, which is the measured value of $\vec{z}$. The steepest descent optimization method is adopted to minimize the cost function. As the result of analysis, variables unavailable in the QAR, such as β, p, q and r, are capable of being estimated.

The above-mentioned unavailable variables in the QAR, need initial values as a basis for correction, where the angular rates, such as p, q, r, are obtained from derivatives of ϕ, θ, and Ψ with time by using the method of monotonic cubic interpolation. This interpolation method is used to connect the flight data into a continuous curve to obtain the slope of the curve. The value of β cannot be obtained from the derivative. The initial value of β is assumed to be 0 at the time of estimation, and it is calculated when the Eq. 2.6 is satisfied.

Aircraft main geometry and moment of inertia data

The main objective of this article is to present a dynamic stability monitoring method based on the approach of oscillatory motion and eigenvalue motion modes for the twin-jet transport aircraft response to sudden plunging motions. The data of main geometry and moments of inertia are presented in Table 2.1.

Table 2.1 Main geometry and moment of inertia data for the twin-jet transport aircraft

Parameter	twin-jet
Takeoff gross weight (kg)	180,168
Wing reference area, S (m^2)	361.300
Mean chord length, $\bar{c}$ (m)	6.005
Wing span, b (m)	60.289
Moment of inertia-x axis, I_{xx} ($kg \cdot m^2$)	12,815,012

Moment of inertia-y axis, I_{yy} (kg·m^2)	12,511,197
Moment of inertia-z axis, I_{zz} (kg·m^2)	53,650,986
Moment of inertia-xz axes, I_{xz} (kg·m^2)	0.0

Non-linear and Unsteady Aerodynamic Database

The actual physical phenomenon of an aircraft flying in the atmosphere is the physical movement along the flight trajectory over time. Since all flight variables recorded are based on the body axes, it is more convenient to estimate the force and moment coefficients for aircraft on the same axes system as follows (Roskam 2018):

1) force coefficients acting on the body axes of the aircraft

$$ma_x = C_x \bar{q} S + T_x \tag{2.12}$$

$$ma_y = C_y \bar{q} S + T_y \tag{2.13}$$

$$ma_z = C_z \bar{q} S + T_z \tag{2.14}$$

2) moment coefficients about the body axes of the aircraft

$$C_l \bar{q}\, S\, b = I_{xx}\, \dot{p} - I_{xz}\, \dot{r} + qr(I_{zz} - I_{yy}) - I_{xz}\, pq \tag{2.15}$$

$$C_m \bar{q}\, S \bar{c} = I_{yy}\, \dot{q} + rp(I_{xx} - I_{zz}) + I_{xz}\,(p^2 - r^2) - T_m \tag{2.16}$$

$$C_n \bar{q}\, S\, b = -I_{xz}\, \dot{p} + I_{zz}\, \dot{r} + pq(I_{yy} - I_{xx}) + I_{xz} qr \tag{2.17}$$

where m is the aircraft mass; $\bar{q}$ is the dynamic pressure; S is the wing reference area; C_x, C_z, and C_m are the longitudinal aerodynamic force and moment coefficients; C_y, C_l, and C_n are the lateral-directional aerodynamic force and moment coefficients; and I_{xx}, I_{yy}, and I_{zz} are the moments of inertia about x-, y-, and z-axes, respectively. The products of inertia, I_{xy}, I_{xz}, and I_{yz}, are assumed zero in the present case; but are included in the equations because non-zero values may be available in other applications. The terms, T_x, T_y, T_z, and T_m, represent the thrust contributions to the force in the direction of x-, y-, z-axes, and to the pitching moment, respectively.

In equations (2.15) ~ (2.17), pq, qr, pr are the product terms of two dependent variables or p^2, r^2 are the square terms of a variable; those are non-linear terms in mathematics. Therefore, equations (2.15) to (2.17) belong to the nonlinear differential equation system. Non-linear differential equations

are very difficult to solve mathematically, and the physical phenomena of motion are more complicated (Fazelzadeh and Sadat-Hoseini 2012). In the physical sense, the product term of the two dependent variables is related to each other, which is the coupling effect of nonlinear motion. The raw flight data of QAR or FDR can be used to establish a non-linear and unsteady aerodynamic database through the steps of flowchart in Fig. 2.1.

The terms on the left-hand side of Eqs. (2.15) - (2.17) are rolling, pitching, and yawing moments, respectively. The moments due to inertia coupling on the right-hand side in Eqs. (2.15) - (2.17) will be produced due to the abrupt change in the flight attitude before and during the severe clear-air turbulence encounters.

Development of nonlinear and unsteady aerodynamic models

This section describes the development process of nonlinear and unsteady aerodynamic models, as shown in Fig. 2.2. The flowchart of Fig. 2.2 is based on the data of the non-linear and unsteady aerodynamic database; the thrust data in aerodynamic database has been separated from aerodynamic coefficienties; Model strucg-n, the numerical model structure, is setup through parameter selection, time segment selection, sampling rate setting, and then go through the refining process of fuzzy-logic modeling to establish the required models; the operational efficiency enhancement can be studied after of model defuzzification.

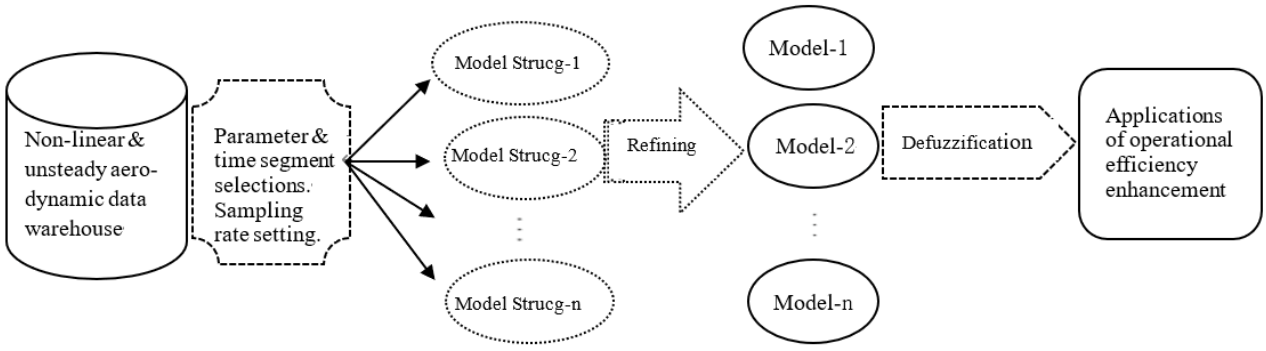

Fig. 2.2 Flowchart for development of non-linear and unsteady aerodynamic models

T_x, T_y, T_z, T_m are the axial thrusts along body x-, y-, z-coordinate, and pitching moment about y-axis, respectively, in the equations (2.12) ~ (2.14), and (2.16). It can be known from the various thrusts that the force and moment acting on the aircraft will be affected by the engines. Both thrust and

aerodynamic forces are generated together, and the two effects cannot be accurately separated only from the flight record data during analysis. To accurately estimate the aerodynamic coefficient, it is necessary to obtain an accurate thrust value to separate the thrust effects, and then the accurate aerodynamic coefficients can be obtained (Lan et al. 2012).

Since the values of thrust for aircraft in flight cannot be directly measured in the current state of the art, they are neither recorded in the QAR nor FDR. The manufacturers of engines agreed that using such parameters as the Mach number, airspeed, flight altitude, temperature, rpm of the pressure compressors, and engine pressure ratios are adequate to estimate the engine thrust (Chang 2014). To study aircraft performance with fuel consumption, data from the flight manual for the fuel flow rate ($\dot{m}_f$) at various altitude (h), weight (W), Mach number (M), calibrated airspeed (CAS), engine pressure ratio (EPR), in cruise flight are utilized.

For the Pratt & Whitney turbofan engines, thrust (T) is defined by EPR, so that the thrust model is set up as:

$$T = f(h, W, M, \text{CAS}, \text{EPR}, \dot{m}_f) \tag{2.18}$$

For GE or CFM turbofan engines, the rpm of the low-pressure compressor (N_1) is used to set the level of thrust, so that the thrust model is set up as:

$$T = f(h, W, M, \text{CAS}, N_1, \dot{m}_f) \tag{2.19}$$

In the present study, the twin-jet with GE turbofan engines under study will be illustrated. The actual thrust in operation is obtained by using the recorded variables in the QAR, in particular the fuel flow rates. Once the thrust models are generated as a function with the flight conditions of climbing, cruise, and descending phases; one can estimate the thrust magnitude by inserting those flight data into the aerodynamic database.

When studying the nonlinear and unsteady aerodynamic characteristics of motion, it can be found that the nonlinear and unsteady aerodynamics with hysteresis (Chang et al. 2010; Lan and Chang 2018; Paziresh et al. 2017) are affected by many parameters of motion state. The aerodynamic models

developed by the fuzzy-logic modeling method is very suitable for aerodynamic research of coupling motion, and can be used to enchance the operational efficiency of transport aircraft. The development process of nonlinear and unsteady aerodynamic models are shown in Fig. 2.2.

Modeling means to establish the numerical relationship among certain variables of interest. In the fuzzy-logic model, more complete necessary influencing flight variables can be included to capture all possible effects on aircraft response to structure deformations. The longitudinal main aerodynamics is assumed to depend on the following ten flight variables(Chang et al. 2010):

$$C_x,\ C_z,\ C_m = f(\alpha, \dot{\alpha}, q, k_1, \beta, \delta_e, M, p, \delta_s, \bar{q}) \tag{2.20}$$

The coefficients on the left-hand side of Eq. (2.20) represent the coefficients of axial force (C_x), normal force (C_z), and pitching moment (C_m), respectively. The variables on the right hand side of Eq. (2.20) denote the angle of attack (α), time rate of angle of attack ($d\alpha/dt$, or $\dot{\alpha}$), pitch rate (q), longitudinal reduced frequency (k_1), sideslip angle (β), control deflection angle of elevator (δ_e), Mach number (M), roll rate (p), stabilizer angle (δ_s), and dynamic pressure ($\bar{q}$). These variables are called the influencing variables. The roll rate is included here because it is known that an aircraft encountering hazardous weather tend to develop rolling which may affect longitudinal stability. The variable of dynamic pressure is for estimation of the significance in structural deformation effects.

For the lateral-directional aerodynamics (Chang et al. 2010),

$$C_y,\ C_l,\ C_n = f(\alpha, \beta, \phi, p, r, k_2, \delta_a, \delta_r, M, \dot{\alpha}, \dot{\beta}) \tag{2.21}$$

The coefficients on the left-hand side of Eq. (2.21) represent the coefficients of side force (C_y), rolling moment (C_l) and yawing moment (C_n), respectively. The variables on the right-hand side of Eq. (2.21) denote the angle of attack (α), sideslip angle (β), roll angle (ϕ), roll rate (p), yaw rate (r), lateral-directional reduced frequency (k_2), control deflection angle of aileron (δ_a), control deflection angle of rudder (δ_r), Mach number (M), the time rate of angle of attack ($\dot{\alpha}$), and the time rate of sideslip angle ($\dot{\beta}$).

The most representative of numerical differentiation theory is the difference method. This paper uses the central difference method to take the derivative. The central difference method to obtain the derivative is to take the differential point as the center point, and respectively select a value close to 0 from the left and right of the differential point to compare, and obtain the derivative of the certain point.

Assuming a function f(x), if one wants to find the derivative at the point x, take x as the center point and select the value of the distance between the left and right sides close to 0, namely f(x+) and f(x-), and then find the Taylor expansion and the principle of the central difference method are as follows:

Taylor expansion to find f(x+ Δx):

$$f(x+\Delta x) = f(x) + f'(x)\Delta x + \frac{f^{(2)}(x)}{2}\Delta x^2 + ... \tag{2.22}$$

Taylor expansion to find f(x- Δx):

$$f(x-\Delta x) = f(x) + f'(x)(-\Delta x) + \frac{f^{(2)}(x)}{2}(-\Delta x)^2 + ...$$

$$f(x-\Delta x) = f(x) - f'(x)\Delta x + \frac{f^{(2)}(x)}{2}\Delta x^2 + ...$$

Subtracting (2.22) from (2.23), one gets

$$f(x+\Delta x) - f(x-\Delta x) = 2f'(x)\Delta x$$

$$f'(x) = \frac{f(x+\Delta x) - f(x-\Delta x)}{2\Delta x}$$

Although the above-mentioned numerical differentiation method is used to obtain the derivative of a certain point of the function curve, in fact, it can also be applied to the derivative analysis of experimental data. However, the experimental data are scattered and discontinuous points, and interpolation must be used to connect the points into a continuous curve. Fuzzy-logic modeling plays the function of interpolation.

The tangent slope of a point on the curve is the derivative value of this point. Add and subtract a small same value to the abscissa value of this point respectively, corresponding to the slope of the line connecting two points on the curve, which is calculated by the finite difference method. Fuzzy-logic modeling is extremely important in the aerodynamic performance analysis of actual flight data. Here are two examples of applying the fuzzy-logic modeling model to take derivatives:

The longitudinal stability derivative ($C_{m\alpha}$) comes from the model of C_m. The aerodynamic derivative of the unsteady aerodynamic model can be calculated using the central interpolation method. The formula of the central difference method is as follows:

$$C_{m\alpha} = [C_m(\alpha + \Delta\alpha, ---) - C_m(\alpha - \Delta\alpha, ---)]/2\Delta\alpha \quad (2.25)$$

$\Delta\alpha$ =0.1 degrees mean that α changes up and down by 0.1 degrees, while all other variables remain unchanged.

The damping derivative (C_{lp}) is proposed from the model C_l. The formula of the central interpolation method is as follows:

$$C_{lp} = [C_l(---, p + \Delta p, ---) - C_l(---, p - \Delta p, ---)]/2\Delta p \quad (2.26)$$

Where Δp is in unit of deg/sec.

The calculations of all other aerodynamic derivatives are derived from the same method in this paper.

Flight Simulation

Since the rapid changes of aerodynamic forces and moments in turbulence, it is difficult to identify the individual modes of motion from these eigenvalues through digital 6-DOF flight simulations from one instant to another. Regarding to the dynamic stability monitoring, one approach to solve this problem is to use the approximate modes of motion obtained from decoupled longitudinal and lateral-directional equations as guidance.

The decoupled linearized longitudinal equations of motion, which are decoupled from the lateral-directional motions in reference of (Roskam 2018) are given by

$$\dot{u} = -g\theta\cos\theta_1 + X_u u + X_\alpha \alpha + X_{\delta e}\delta e \quad (2.27)$$

$$U_1\dot{\alpha} - U_1\dot{\theta} = -g\theta\sin\theta_1 + Z_u u + Z_\alpha \alpha + Z_{\dot{\alpha}}\dot{\alpha} + Z_q\dot{\theta} + Z_{\delta e}\delta e \quad (2.28)$$

$$\ddot{\theta} = M_u u + M_\alpha \alpha + M_{\dot{\alpha}}\dot{\alpha} + M_q\dot{\theta} + M_{\delta e}\delta e \quad (2.29)$$

where the X_u, X_α, and $X_{\delta e}$ are the dimensional variations of force along X axis with the speed, angle of attack, and elevator angle, respectively; the other dimensional derivatives of Z and M are described and given in reference of (Roskam 2018). The decoupled lateral-directional equations of motion are:

$$U_1\dot{\beta} + U_1\dot{\psi} = g\phi\cos\theta_1 + Y_\beta\beta + Y_p\dot{\phi} + Y_r\dot{\psi} + Y_{\delta a}\delta a + Y_{\delta r}\delta r \quad (2.30)$$

$$\ddot{\phi} - \overline{A}_1\ddot{\psi} = L_\beta\beta + L_p\dot{\phi} + L_r\dot{\psi} + L_{\delta a}\delta a + L_{\delta r}\delta r \quad (2.31)$$

$$\ddot{\psi} - \overline{B}_1\ddot{\phi} = N_\beta\beta + N_p\dot{\phi} + N_r\dot{\psi} + N_{\delta a}\delta a + N_{\delta r}\delta r \quad (2.32)$$

where $\overline{A}_1 = I_{xz} / I_{xx}$ and $\overline{B}_1 = I_{xz} / I_{zz}$; the dimensional derivatives of *Y*, *L*, and *N* are described and given in reference of (Roskam 2018). The characteristic equations for Eqs, (2.27) ~ (2.29), and Eqs. (2.30) ~ (2.32) are polynomials of the 4th degree and their roots are solved with a quadratic factoring method based on the Lin-Bairstow algorithm in reference of (Hovanessian and Pipes 1969).

The 4th degree polynomial of longitudinal characteristic equations has 4 roots; they are two complex conjugates (Lan and Chang 2012). The short-period mode is one of the two complex conjugates. Another one is the phugoid mode (long period mode). Each mode has the same real part, but with imaginary parts of equal magnitude and opposite signs. The 4th degree polynomial of lateral-directional characteristic equations also has 4 roots; they are one pair of complex conjugates and two real values. The pair of complex conjugates represent the dutch roll mode. One of two real values represent the spiral mode and another one represents the roll mode.

Fuzzy-logic Modeling Algorithm

Modelling procedures start from setting up numerical relations between the input (i.e. flight variables) and output (i.e. flight operations or aircraft response). To obtain continuous variations of predicted results, the present method is based on the internal functions, instead of fuzzy sets (Karasan et al. 2018), to generate the output of the model.

The fuzzy-logic algorithm can take advantage of correlating multiple parameters without assuming explicit functional relations among them (Dang et al. 2017; Shi et al. 2017). The algorithm employs many internal functions to represent the contributions of fuzzy cells (to be defined later) to the over-all prediction. The internal functions are assumed to be linear functions of input parameters as follows (Weng et al. 2006):

$$P^i = y_i(x_1, x_2, \cdots, x_r, \cdots x_k) = p_0^i + p_1^i x_1 + \cdots + p_r^i x_r + \cdots p_k^i x_k \tag{2.30}$$

where p_r^i, r =0, 1, 2,…, k, are the coefficients of internal functions y_i, and k is number of input variables. In Eq. 1, y_i is the estimated aerodynamic coefficient of force or moment, and x_r are the variables of the input data. The numbers of the internal functions (i.e. cell's numbers) are quantified by the membership functions.

With the internal function chosen in a linear form, the fuzzy-logic model resembles the multiple linear regression method. What makes the fuzzy-logic model unique is that it is in a form of fuzzy

cell structure composed of linear equations. In other words, there are different numbers of cells corresponding with each input parameter. The values of each fuzzy variable, such as the angle of attack, are divided into several ranges, each of which represents a membership function (Lan and Chang 2018). The membership functions allow the membership grades of the internal functions for a given set of input variables to be calculated. The ranges of the input variables are all transformed into the domain of [0, 1]. The membership grading also ranges from 0 to 1.0, with "0" meaning no effect from the corresponding internal function, and "1" meaning full effect. Generally, overlapped triangles are frequently the shapes used to represent the grades. A fuzzy cell is formed by taking one membership function from each variable. The output of the fuzzy-logic model is the weighted average of all cell outputs.

There are two main tasks involved in the fuzzy-logic modeling process. One is the determination of coefficients of the linear internal functions. The other is to identify the best structure of fuzzy cells of the model, i.e. to determine the best number of membership functions for each fuzzy variable. The coefficients are calculated with the gradient-descent method by minimizing the sum of squared errors (SSE) (Lan and Chang 2018):

$$SSE = \sum_{j=1}^{m} (\hat{y}_j - y_j)^2 \tag{2.31}$$

On the other hand, the structure of fuzzy cells is optimized by maximizing the multiple correlation coefficients (R^2):

$$R^2 = 1 - \frac{\{\sum_{j=1}^{m} (\hat{y}_j - y_j)^2\}}{\{\sum_{j=1}^{m} (\bar{y} - y_j)^2\}} \tag{2.32}$$

where $\hat{y}_j$ is the output of the fuzzy-logic model, y_j is the measured data, and $\bar{y}$ is the average value of all extracted data.

The aerodynamic model is defined by the values of p_r^i –coefficients. These coefficients are determined by minimizing SSE (Eq. 2.31) with respect to these coefficients. Minimization is achieved

by the gradient-descent method with an iteration formula defined by:

$$p_{r,t+1}^{i} = p_{r,t}^{i} - \alpha_r \frac{\partial(SSE)}{\partial p_r^i} \tag{2.33}$$

where α_r is convergence factor or step size in the gradient method. Since

$$\frac{\partial(SSE)}{\partial p_r^i} = 2\sum_{j=1}^{m}(\hat{y}_j - y_j)\frac{\partial \hat{y}_j(x_{1,j},...,x_{k,j},p_r^1,...,p_k^n)}{\partial p_r^i} \tag{2.34}$$

the computed gradient tends to be small and the convergence is slow. To accelerate the convergence, the iterative formulas are modified by using the local squared errors to give: for r=0,

$$p_{0,t+1}^{i} = p_{0,t}^{i} - 2\alpha_0(\hat{y}_j - y_j)\frac{op[A_1^i(x_{1,j}),...,A_k^i(x_{k,j})]}{\sum_{s=1}^{n} op[A_1^s(x_{1,j}),...,A_k^s(x_{k,j})]} \tag{2.35}$$

and for r = 1, …, k,

$$p_{r,t+1}^{i} = p_{r,t}^{i} - 2\alpha_r(\hat{y}_j - y_j)\frac{op[A_1^i(x_{1,j}),...,A_k^i(x_{k,j})]x_{r,j}}{\sum_{s=1}^{n} op[A_1^s(x_{1,j}),...,A_k^s(x_{k,j})]} \tag{2.36}$$

In Eqs. (2.35) & (2.36), $op[A_1^i(x_{1,j}),...,A_k^i(x_{k,j})]$ is weighted factor of the i^{th} cell; and the index j of the data set, where j=1, 2, …, m, and m is the total number of the data record; and the "*op*" stands product operator of its elements in this paper.

Once the fuzzy-logic aerodynamic models were set up, one can input to the model influencing variables to describe the flight conditions under analysis. In the present paper, all aerodynamic derivatives are computed with central differences through the aerodynamics models.

The fuzzy-logic algorithm can take advantage of correlating multiple parameters without assuming explicit functional relations among them (Chang 2014; Chang et al. 2010). The algorithm employs many internal functions to represent the contributions of fuzzy cells (to be defined later) to the over-all prediction. The internal functions are assumed to be linear functions of input parameters as follows (Roskam 2018):

Numerical Results and Discussions

In the present study, the accuracy of the established unsteady aerodynamic models with six aerodynamic coefficients by using fuzzy-logic modeling technique is estimated by the sum of squared errors (SSE) and the square of multiple correlation coefficients (R^2). All the aerodynamic derivatives in the study of dynamic stability characteristics are calculated with these aerodynamic models of aerodynamic coefficients.

Fig. 3.1 presents the main aerodynamic coefficients of normal force C_z, pitching moment C_m, rolling moment C_l, and yawing moment C_n predicted by the nonlinear and unsteady aerodynamic models. The scattering of C_m-data in Fig. 3.1(b) is most likely caused by turbulence-induced buffeting on the structure, in particular on the horizontal tail. The predicted results of others by the final models have good match with the flight data. Once the aerodynamic models are set up, one can calculate all necessary derivatives by central difference scheme to analyze the stability characteristics.

The final main aerodynamic models of aerodynamic coefficients consist of many fuzzy rules for each coefficient as described from Tables 3.1 and 3.2. In Tables 3.1 and 3.2, the numbers below each input variable represents the number of membership function. The total number of fuzzy cells (n) in each model is the product of each number which presented in column 3. The last column shows the final multiple correlation coefficients (R^2). The accuracy of the established aerodynamic model through the fuzzy-logic algorithm can be judged by the multiple correlation coefficients (R^2).

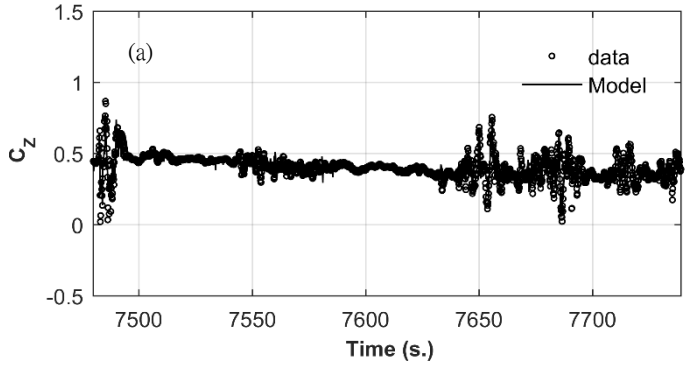

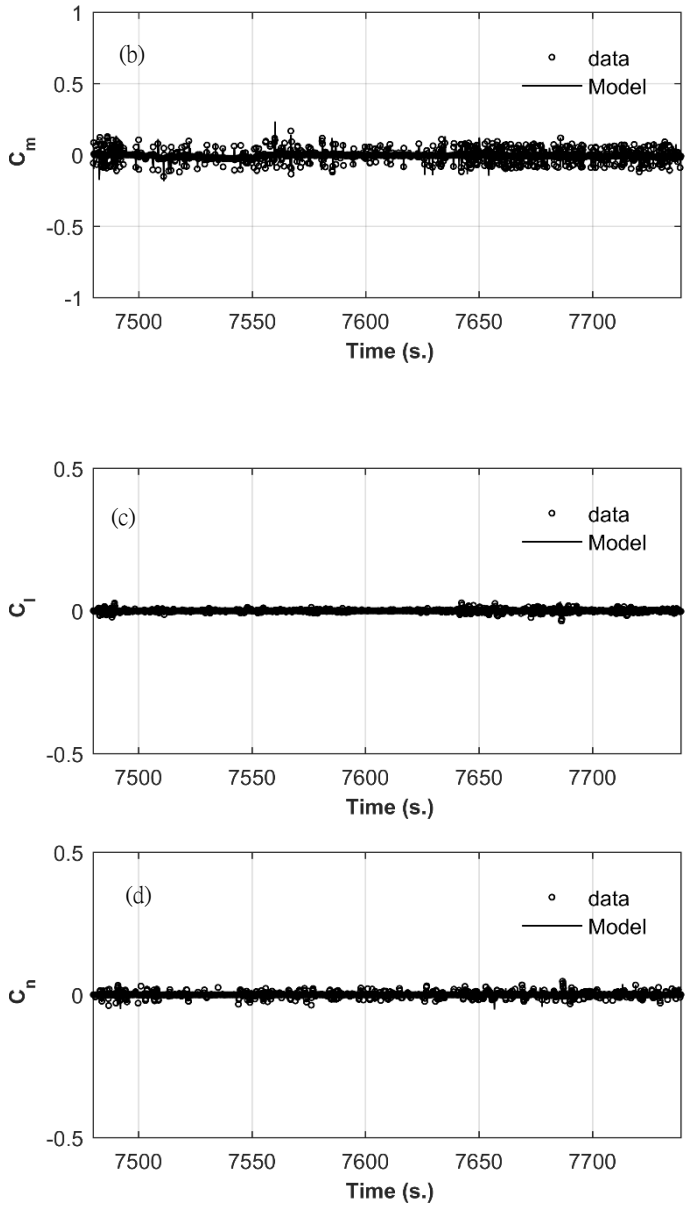

Fig. 3.1 Main aerodynamic coefficients predicted by the nonlinear and unsteady aerodynamic models

Table 3.1 Final main models of longitudinal aerodynamics

Coef.	α , $\dot{\alpha}$, q , k_1 , β , δ_e , M , p , $\overline{q}$									n	R^2
C_z	2	3	3	2	3	3	2	3	2	3888	0.9618
C_m	2	2	3	4	2	3	2	2	3	3456	0.9873

Table 3.2 Final main models of lateral-directional aerodynamics

Coef.										$\dot{\alpha}$	$\dot{\beta}$	n	R^2
C_l	2	3	3	2	2	3	2	2	3	3	2	15552	0.9617

C_n	3	2	4	2	2	2	3	3	2	2	2	13824	0.9435

The twin-jet transport aircraft encountered clear-air turbulences in revenue flights. As a result, several passengers and cabin crews sustained injuries, this event was classified as the aviation accidents. To examine the dynamic stability characteristics, it is imperative to understand the flight environment in detail.

The corresponding flight data for twin-jet transport with plunging motion is presented in Fig. 3.2. The dataset of time span from t=7480~7739 sec used for the modeling are extracted from the FDR. This twin-jet transport encounters severe clear-air turbulence twice during this time span. In Fig. 3.2(a), the variations of normal acceleration (a_z) show the highest a_z being 2.05g around t = 7483 sec and the lowest being-1.05 g around t = 7484 sec in the first turbulence encounter, the highest a_z being 1.91g around t = 7682 sec and the lowest being -0.16 g around t = 7684 sec in the second one. Fig. 3.2(b) shows that variation of α (AOA) is approximately in phase with a_z during those two turbulence encounters; The variation ranges of AOA are 4 deg. to -1.8 deg. in the first turbulence encounter and 5.5 deg. to -2 deg. in the second one. The time history of β is about -2 deg. with the magnitude of small fluctuation, as indicated in Fig 3.2(c). The aircraft rapidly plunges downward during the turbulence encounter. The largest drop-off height reaches 57.3 m in the time span between t = 7484~7486 sec. The Mach number (M) drops from 0.83 to 0.75 in the first turbulence encounter and from 0.80 to 0.70 in the second one, as shown in Fig. 3.2(d).

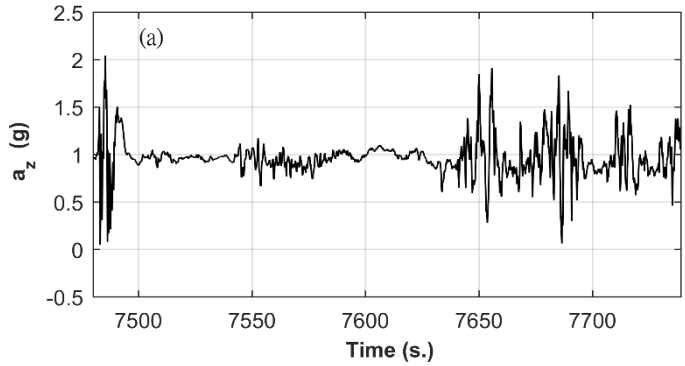

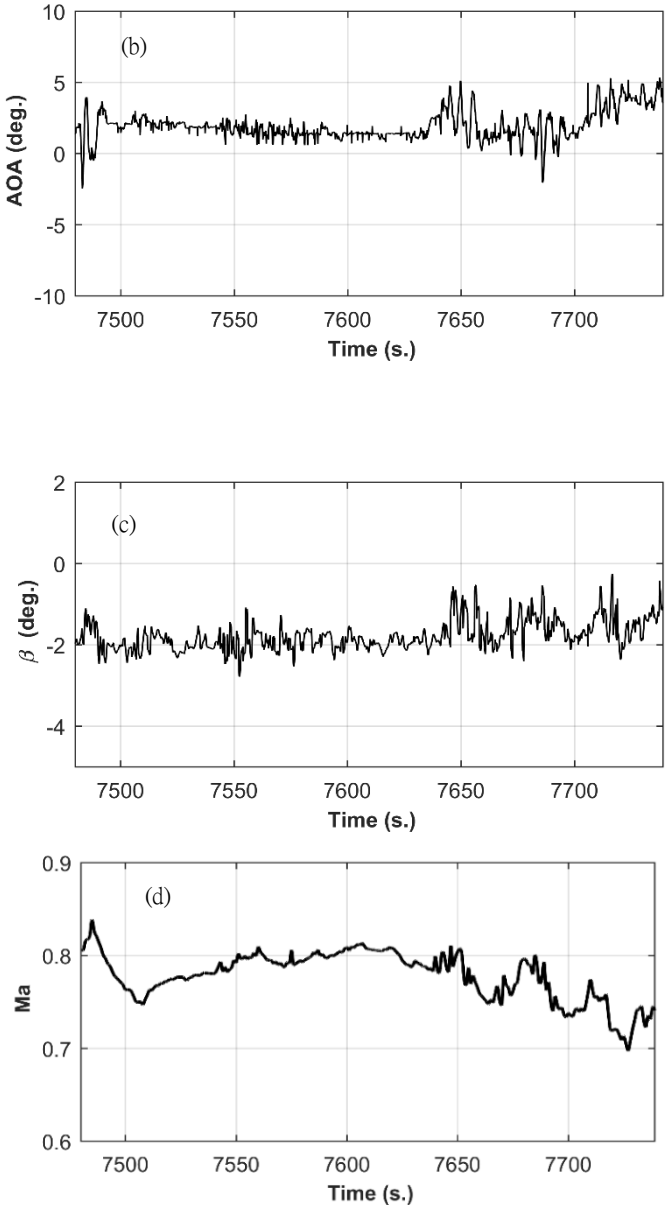

Fig. 3.2 Time history of main flight variables in severe clear-air turbulence

Fig. 3.3 presents the twin-jet transport aircraft response to dynamic flight motion. The magnitudes of pitch rate (q) and roll rate (p) are shown in Fig. 3.3(a); the variation of p is larger than that of q. The yaw rate is not shown because it is small throughout. It implies that pitch angle (θ) does not vary as much as AOA and the variations of roll angle (ϕ) is large, especially during the second turbulence encounter.

Fig. 3.3(b) and 3.3(b) present the time rate of angle of attack ($d\alpha/dt$, or $\dot{\alpha}$) and the time rate of sideslip angle ($\dot{\beta}$), respectively. Fig. 3.3(b) shows that variations of $\dot{\alpha}$ is approximately in phase

with a_z and AOA during those two turbulence encounters. Fig 3.2(c) describes the time history of β is about a certain value with the magnitude of small fluctuation; the variations of roll angle (ϕ) is large; the yaw rate is not shown in Fig. 3.3(a), because it is small throughout. It implies that twin-jet transport aircraft has crosswind encounter, but this crosswind does not have big variations in directions.

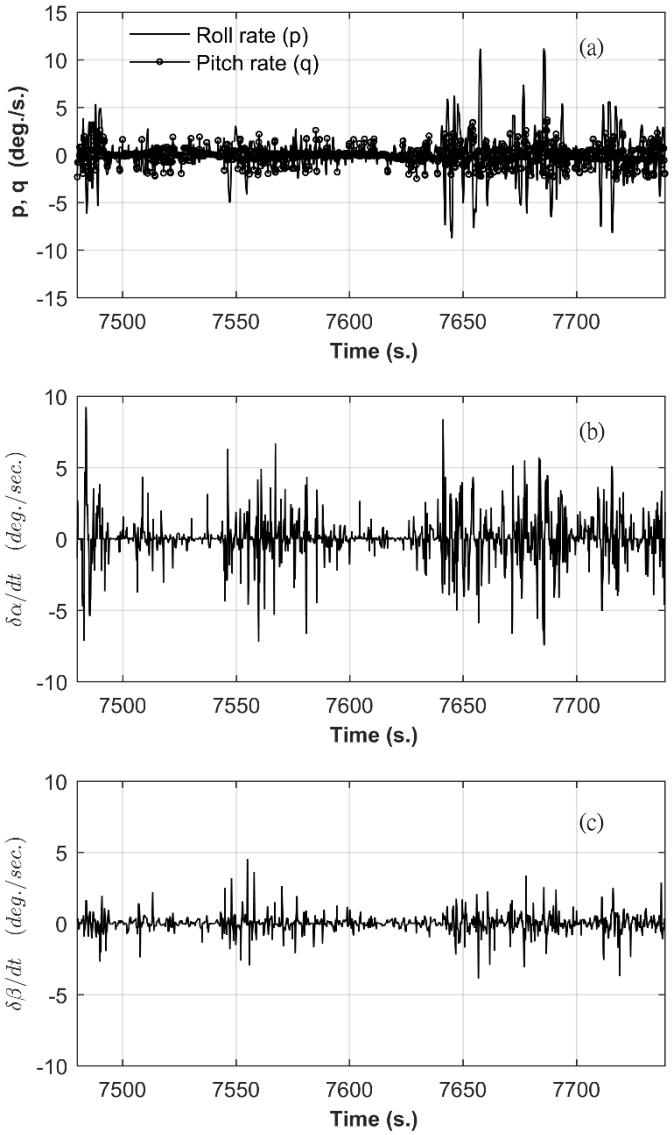

Fig. 3.3 Time history of twin-jet transport aircraft response to dynamic flight motion

In general, the configuration in static stability assessment is based on enough values of steady damping derivatives to keep stable condition. The plunging motion is the biggest factor that easy causes aerodynamic instability, the configuration will produce a time-varying pressure distribution on the surface, which involves the compressibility effect. The longitudinal, roll, and directional

$\dot{\alpha}$ $\dot{\beta}$

$C_{m\dot{\alpha}}$

$C_{z\dot{\alpha}}$

The roll and directional oscillatory derivatives:

$C_{l\dot{\beta}}$ α (3.3)

$C_{n\dot{\beta}}$ α (3.4)

The values of oscillatory derivatives are equivalent to the combinations of steady damping and dynamic derivatives in above Eqs. (3.1) ~ (3.4). The use of oscillatory derivative instead of steady damping only is more consistent with the actual case of plunging motion. To be stable in oscillatory motion, $(C_{zq})_{osc} > 0$, $(C_{mq})_{osc} < 0$, $(C_{lp})_{osc} < 0$, and $(C_{nr})_{osc} < 0$. Physically, if it is unstable, the motion could be divergent in oscillatory motions within a short time period. The values in the period of plunging motion have some differences between oscillatory and steady damping derivatives in Figs 3.4(a) and 3.4(c) due to the effects of the dynamic derivatives (i.e. $\dot{\alpha}$ -derivatives), so as Figs 3.5(a) and 3.5(c) due to the effects of the dynamic derivatives (i.e. $\dot{\beta}$ -derivatives).

Figs 3.4(c),3.4(d) and Figs 3.5(c) show dynamic derivatives of stability. To be stable, $C_{z\dot{\alpha}}$ $C_{m\dot{\alpha}} < 0$, $C_{l\dot{\beta}} < 0$, and $C_{n\dot{\beta}} > 0$. The magnitudes of $C_{z\dot{\alpha}}$ and $C_{m\dot{\alpha}}$ have significant variations and $C_{z\dot{\alpha}} < 0$ in the period of t= 7482.5 ~ 7491 sec in Fig. 3.4(b). It should be noted that $C_{z\dot{\alpha}}$ represents the virtual mass effect and is particularly large in transonic flow to affect the plunging motion (Sheu and Lan 2011). The $(C_{zq})_{osc}$ and $(C_{mq})_{osc}$ are insufficient in oscillatory damping in the periods of t= 7484 ~ 7486 sec and t= 7490~ 7494 sec, as shown in Fig. 3.4(a) and Fig. 3.4(b). The effect of $\dot{\alpha}$ -derivative on $(C_{mq})_{osc}$ is to improve the stability in pitch in the periods of t= 7482.5 ~ 7484 sec and 7486~ 7488.5 sec. The magnitudes of $C_{l\dot{\beta}}$ in Fig. 3.5(c) and $(C_{lp})_{osc}$ in Fig. 3.5(a) are small; C_{lp} is not shown because it is small throughout. The values of $C_{n\dot{\beta}}$ are from positive at t= 7483 sec to negative at t= 7484 sec;

$(C_{nr})_{osc}$ are from positive at t= 7483.5 sec to negative at t= 7485 sec. It implies that the effects of $\dot{\beta}$-derivative is to cause the directional stability more unstable.

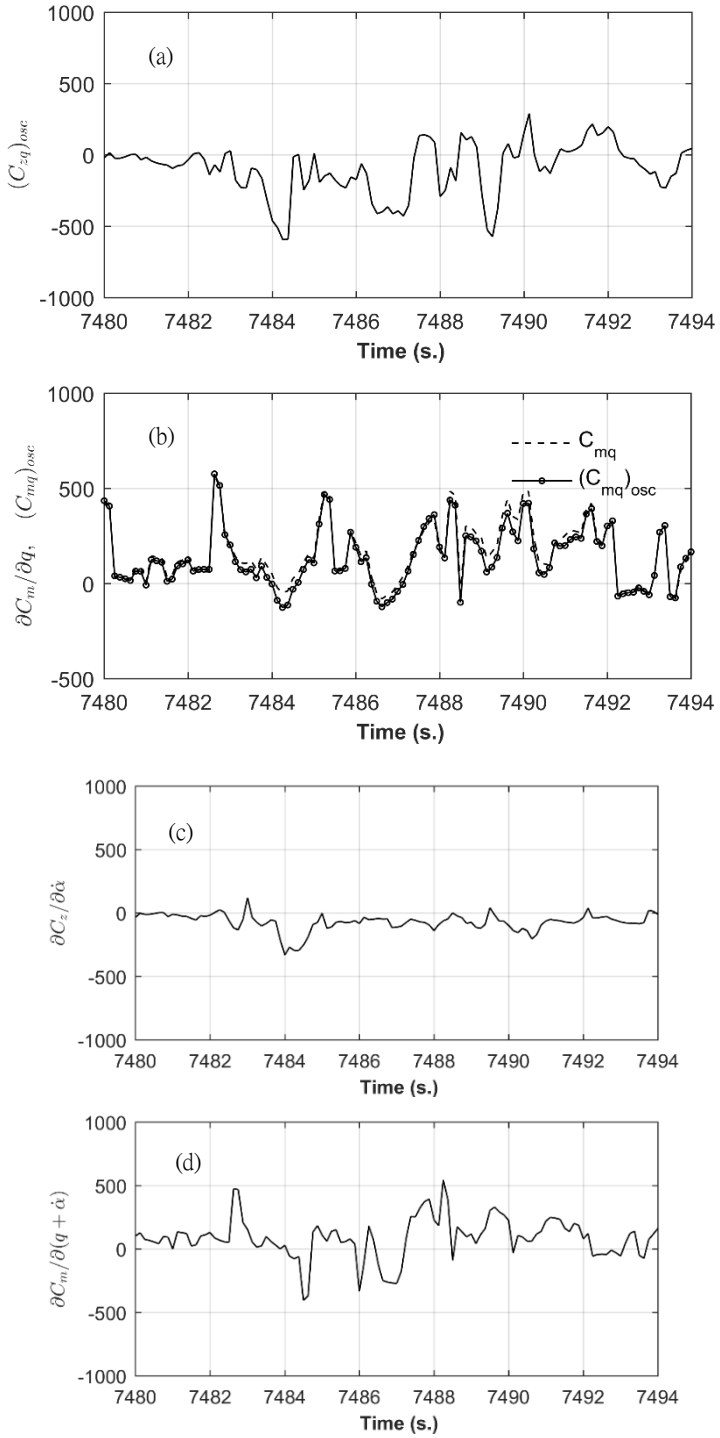

Fig. 3.4 Time history of main longitudinal oscillatory derivatives along the flight path

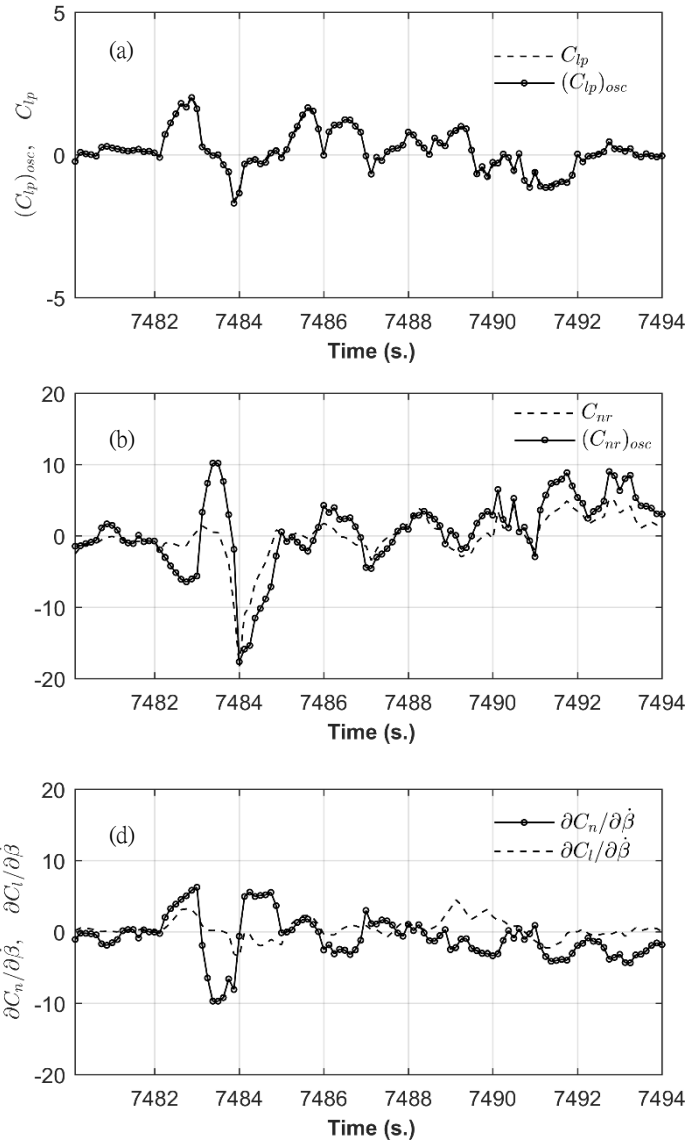

Fig. 3.5 Time history of main lateral-directional oscillatory derivatives along the flight path

In essence, the effects of $\dot{\alpha}$ -derivative on $(C_{zq})_{osc}$, and $\dot{\beta}$ -derivative on $(C_{lp})_{osc}$ are small in Figs 3.4 and 3.5. However, the effect of $\dot{\alpha}$ -derivative on $(C_{mq})_{osc}$ is to improve the stability in pitch; while the effects of $\dot{\beta}$ -derivative is to cause more directional instability. These results indicate that the turbulent crosswind has some adverse effects on directional stability and damping. Although the dynamic derivatives tend to be small for the present configuration, these are much helpful to understand the unknown factors of instability characteristics.

In the present study, the longitudinal and lateral-directional motion modes are analyzed based on the damping ratio (ζ) and undamped natural frequency (ω_n). The roots of the complex conjugate are as follows:

$$\lambda_{1,2} = -\zeta\omega_n \pm i\omega_n\sqrt{1-\zeta^2} \tag{3.5}$$

where $-\zeta\omega_n$ is real part (i.e. in-phase) and $\pm i\omega_n\sqrt{1-\zeta^2}$ are imaginary (i.e. out-of-phase) parts. λ_r and λ_i represent eigenvalues of real and imaginary parts, respectively. If λ_r is positive, the system is unstable; if it is negative, the system is stable (Chang et al. 2009).

Fig. 3.6 presents the eigenvalues of the short-period and phugoid modes. The eigenvalues of real part in Fig. 3.6(a) are in small negative, except two portions at t= 7486.2 sec and t= 7492.0 ~7493.0 sec in small positive. The short period mode is typically a damped oscillation in pitch about the body y-axis in normal flight conditions. The short period mode is mostly in stable condition due to the value of $(C_{mq})_{osc}$ being mostly negative to have adequate pitch damping in oscillatory motions in the time span between t = 7484~7486 sec with largest drop-off height, the highest a_z being 2.05g around t = 7483 sec and the lowest being -1.05 g around t = 7484 sec in Fig. 3.2(a), highest AOA about 4 deg. in Fig. 3.2(b). The eigenvalues of real part in Fig. 3.6(b) are positive and the magnitude varies like a mountain chain with pinnacle. The value of $(C_{zq})_{osc}$ is in negative and the magnitudes of $C_{z\dot{\alpha}}$ are also in negative values; $(C_{zq})_{osc}$ is insufficient in oscillatory damping and with virtual mass effects during sudden plunging motion to cause the phugoid mode in unstable condition. Note that part of the conventional phugoid mode has degenerated into the plunging mode.

Fig. 3.7 presents the eigenvalues of the Dutch roll, spiral, and roll modes. The eigenvalues of real part in Fig. 3.7(a) are positive in the time period of t= 7490~7494 sec. and all values in Fig. 3.7(b) are also positive, except the value of small portion at t= 7484 sec. The values of $(C_{nr})_{osc}$ are mostly positive; while $(C_{nr})_{osc}$ is insufficient in oscillatory damping to induce the unstable Dutch roll and spiral modes. The eigenvalues of real part in Fig. 3.7(c) are negative. The roll mode is stable because the values of $(C_{lp})_{osc}$ are mostly small negative to have some roll damping.

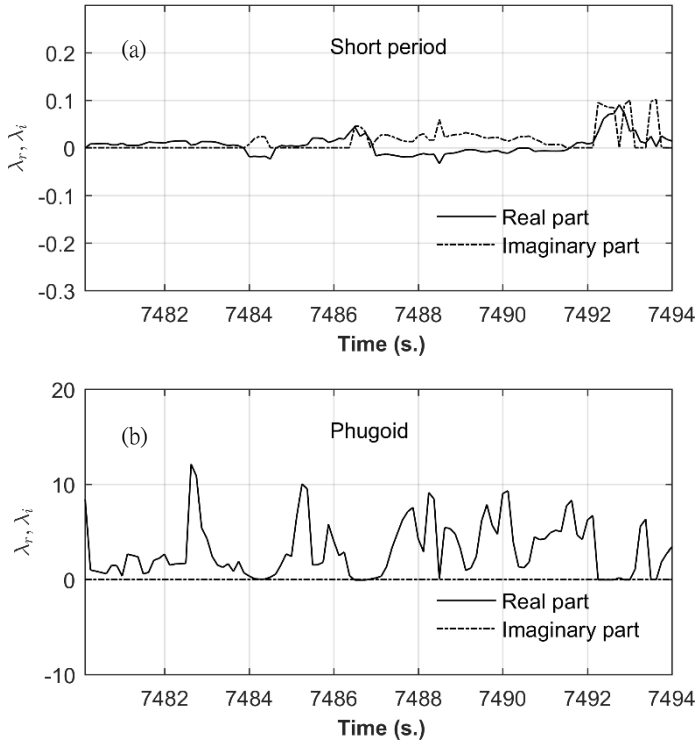

Fig. 3.6 Eigenvalues of longitudinal modes of motion

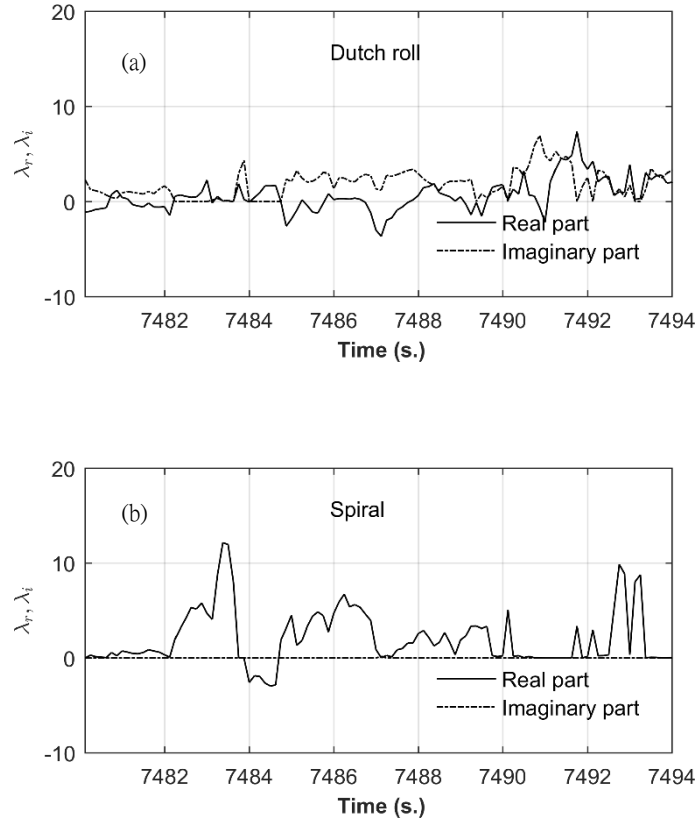

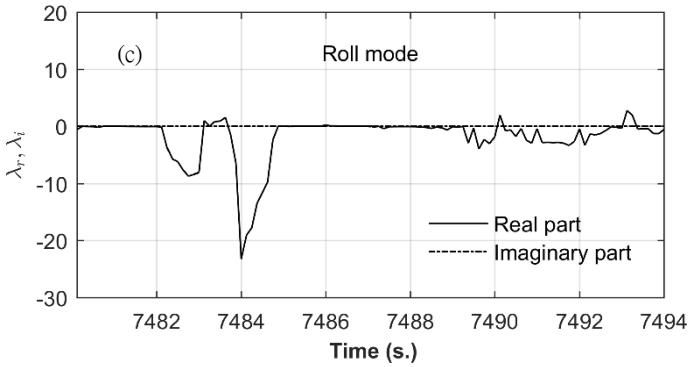

Fig. 3.7 Eigenvalues of lateral-directional modes of motion

Airlines care about is the vertical plunging mode of motion which is not considered in the classical flight dynamics. According to (Sheu and Lan 2011), in vertical plunging motion the damping term is mainly related to $C_{z\dot{\alpha}}$. It may be possible to define the severity of plunging motion based on the vertical plunging equation of motion.

For the present purpose, if the severity is defined by the lowest load factor developed, then this transport aircraft developed -1.05g with Δh=57.3m (around t = 7483 sec). The phugoid mode in Fig. 3.6(b) has all positive real eigenvalues; it implies insufficient in longitudinal oscillatory damping and with virtual mass effects during sudden plunging motion. So as this transport does not have sufficient lateral-directional oscillatory damping. Therefore, it may be concluded that the plunging motion is more severe because of its unstable condition.

Concluding Remarks

The main objective of this paper was to present a dynamic stability monitoring method based on the approach of oscillatory motion and eigenvalue motion modes for jet transport aircraft response to sudden plunging motions. Three obvious achievements could be concluded from the present paper as follows:

1) The flight data mining and the fuzzy-logic modeling techniques were shown to be effective in establishing the nonlinear and dynamic aerodynamic models through the flight data of FDR. The fuzzy-logic aerodynamic models had robustness and nonlinear interpolation capability to generate the required independent variables in predicting the oscillatory motion during severe clear-air

turbulence encounter.

2) The eigenvalues of both longitudinal and lateral-directional motion modes were analyzed through digital flight simulation based on decoupled dynamic equations of motion. The decoupled concept was an innovative consideration for the flight simulation of six-DOF.

3) The results of flight simulation showed that the Phugoid, Dutch roll, and spiral modes were in unstable conditions for the present study transport aircraft. Those unstable conditions were easily judged by the positive real part of the eigenvalues during sudden plunging motion.

The oscillatory motion and eigenvalue approaches for the dynamic stability assessments were much helpful to understand the effects of severe clear-air turbulence encounter on dynamic stability characteristics. The simulated results could provide the training program of loss control prevention for the airlines to enhance aviation safety and operational efficiency.

Acknowledgments

This work was supported in part by the Joint Funds project of the National Natural Science Foundation of China (grant no. U1733203), the special key projects of technological innovation and application development of Chongqing (grant no. cstc2019jscx-fxydX0036), and the scientific research project of CQJTU (grant no. 19JDKJC-A012).

Nomenclature

a_z = normal accelerations, g

b = wing span, m

C_x, C_z, C_m = longitudinal aerodynamic force and moment coefficients

C_y, C_l, C_n = lateral-directional aerodynamic force and moment coefficients

$\bar{c}$ = mean aerodynamic chord, m

h = altitude, m

I_{xx}, I_{yy}, I_{zz} = moments of inertia about x-, y-, and z-axes, respectively, kg·m^2

I_{xy}, I_{xz}, I_{yz} = products of inertia, kg·m^2

k_1, k_2 = longitudinal and lateral-directional reduced frequencies, respectively

L, M, N = moments acting along the (x,y,z)-body axes of aircraft, respectively, N·m

M = Mach number

m = aircraft mass, kg

$\dot{m}_f$ = fuel flow rate, kg/hr

N_1 = the rpm of the compressor, rpm

p, q, r = body-axis roll rate, pitch rate, and yaw rate, deg./s.

$\bar{q}$ = dynamic pressure, kpa

S = wing reference area, m^2

T, W = thrust and aircraft weight in flight, N, respectively

T_2 = time to double or halve the amplitude, sec.

t = time, sec.

X, Y, Z = forces acting on the aircraft body-fixed axes about x-, y-, and z-axes, N, respectively

$\alpha, \dot{\alpha}$ = angle of attack, deg. and time rate of angle of attack, deg./sec., respectively

$\beta, \dot{\beta}$ = sideslip angle, deg. and time rate of sideslip angle, deg./sec., respectively

$\delta_a, \delta_e, \delta_r$ = control deflection angles of aileron, elevator and rudder, respectively, deg.

ϕ, θ, ψ = Euler angles in roll, pitch, and yaw, respectively, deg.

λ_r, λ_i = eigenvalue in real (i.e. in-phase) and imaginary (i.e. out-of-phase) parts, respectively.

ζ = damping ratio

ω_n = natural frequency

References

Chang, R. C. (2014). "Performance diagnosis for turbojet engines based on flight data." *Journal of Aerospace Engineering*, 27(1), 9-15.

Chang, R. C., and Tan, S. (2013). "Examination of dynamic aerodynamic effects for transport aircraft with hazardous weather conditions." *Journal of Aeronautics, Astronautics and Aviation*, 45(1), 51-62.

Chang, R. C., Ye, C.-E., Lan, C. E., and Guan, M. (2009). "Flying qualities for a twin-jet transport in severe atmospheric turbulence." *Journal of Aircraft*, 46(5), 1673-1680.

Chang, R. C., Ye, C.-E., Lan, C. E., and Guan, W.-L. (2010). "Stability characteristics for transport aircraft response to clear-air turbulence." *Journal of Aerospace Engineering*, 23(3), 197-204.

Dang, Q. V., Vermeiren, L., Dequidt, A., and Dambrine, M. (2017). "Robust stabilizing controller design for TakagiSugeno fuzzy descriptor systems under state constraints and actuator saturation." *Fuzzy Sets and Systems*, 329, 77-90.

Fazelzadeh, S. A., and Sadat-Hoseini, H. (2012). "Nonlinear flight dynamics of a flexible aircraft subjected to aeroelastic and gust loads." *Journal of Aerospace Engineering*, 25(1), 51-63.

Hamilton, D. W., and Proctor, F. H. "An aircraft encounter with turbulence in the vicinity of a thunderstorm." *Proc., 21st AIAA Applied Aerodynamics Conference 2003, June 23, 2003 - June 26, 2003*, AIAA International.

Han, J., Kamber, M., and Pei, J. (2011). *Data Mining: Concepts and Techniques, 3rd ed*, Morgan Kaufmann Publishers, USA.

Hovanessian, S. A., and Pipes, L. A. (1969). *Digital Computer Methods in Engineering*, McGraw-Hill Book Company.

Karasan, A., Ilbahar, E., Cebi, S., and Kahraman, C. (2018). "A new risk assessment approach: Safety and Critical Effect Analysis (SCEA) and its extension with Pythagorean fuzzy sets." *Safety Science*, 108, 173-187.

Lan, C. E., and Chang, R. C. (2012). "Fuzzy-Logic Analysis of the FDR Data of a Transport Aircraft in Atmospheric Turbulence." *London: Intech Open* 119-146.

Lan, C. E., and Chang, R. C. (2018). "Unsteady aerodynamic effects in landing operation of transport aircraft and controllability with fuzzy-logic dynamic inversion." *Aerospace Science and Technology*, 78, 354-363.

Lan, C. E., and Guan, M. "Flight dynamic analysis of a turboprop transport airplane in icing accident." *Proc., AIAA Atmospheric Flight Mechanics Conference 2005, August 15, 2005 - August 18, 2005*, American Institute of Aeronautics and Astronautics Inc., 551-569.

Lan, C. E., Wu, K., and Yu, J. (2012). "Flight Characteristics Analysis Based on QAR Data of a Jet Transport During Landing at a High-altitude Airport." *Chinese Journal of Aeronautics*, 25(1), 13-24.

Lee, Y.-N., and Lan, C. E. (2000). "Analysis of random gust response with nonlinear unsteady aerodynamics." *AIAA journal*, 38(8), 1305-1312.

Min, C.-O., Lee, D.-W., Cho, K.-R., Jo, S.-J., Yang, J.-S., and Lee, W.-B. (2011). "Control of approach and landing phase for reentry vehicle using fuzzy logic." *Aerospace Science and Technology*, 15(4), 269-282.

Paziresh, A., Nikseresht, A. H., and Moradi, H. (2017). "Wing-Body and Vertical Tail Interference Effects on Downwash Rate of the Horizontal Tail in Subsonic Flow." *Journal of Aerospace Engineering*, 30(4).

Roskam, J. (2018). *Airplane Flight Dynamics and Automatic Flight Controls*, DARcorporation, Lawrence, Kansas.

Sauer, M., Steiner, M., Sharman, R. D., Pinto, J. O., and Deierling, W. K. (2019). "Tradeoffs for routing flights in view of multiple weather hazards." *Journal of Air Transportation*, 27(2), 70-80.

Sheu, D., and Lan, C.-T. (2011). "Estimation of turbulent vertical velocity from nonlinear simulations of aircraft response." *Journal of Aircraft*, 48(2), 645-651.

Shi, K., Wang, B., Yang, L., Jian, S., and Bi, J. (2017). "TakagiSugeno fuzzy generalized predictive control for a class of nonlinear systems." *Nonlinear Dynamics*, 89(1), 169-177.

Thompson, D., Mogili, P., Chalasani, S., Addy, H., and Choo, Y. "A computational icing effects

study for a three-dimensional wing: Comparison with experimental data and investigation of spanwise variation." *Proc., 42nd AIAA Aerospace Sciences Meeting and Exhibit, January 5, 2004 - January 8, 2004*, American Institute of Aeronautics and Astronautics Inc., 5470-5496.

Wang, Y., Liu, P., Hu, T., and Qu, Q. (2016). "Investigation of co-rotating vortex merger in ground proximity." *Aerospace Science and Technology*, 53, 116-127.

Weng, C.-T., Ho, C.-S., Edward Lan, C., and Guan, M. (2006). "Aerodynamic analysis of a jet transport in windshear encounter during landing." *Journal of Aircraft*, 43(2), 419-427.

Wolberg, G., and Alfy, I. (2002). "An energy-minimization framework for monotonic cubic spline interpolation." *Journal of Computational and Applied Mathematics*, 143(2)(2), 145-188.